Interaction of Quantized Vortex Rings with Quantized Vortex Lines in Rotating He II†

K. W. SCHWARZ
Department of Physics and James Franck Institute, University of Chicago, Chicago, Illinois
(Received 29 May 1967)

The effect of steady rotation on a beam of charged vortex rings in He II has been investigated. The rotation-dependent changes in the beam are interpreted in terms of strong ring-line interactions experienced by a fraction of the rings, plus collective effects which are the same for all rings. An approximate calculation based on inviscid hydrodynamics and a uniform distribution of vortex lines yields fair agreement with the observed behavior.

I. INTRODUCTION

THE quantum nature of the superfluid seems to require that vorticity exist only in the form of quantized vortex lines and vortex sheets. In all other respects, the large-scale behavior appears to be that of a perfect fluid. These ideas have been accepted for some time, mainly on phenomenological grounds since no wholly adequate theoretical description has been achieved. However, the recent advances in treating the weakly interacting Bose gas indicate that they are sound also from a fundamental point of view.[1–4] In any case, there is no doubt that the quantized vortex line model has been quite successful in explaining the odd properties of the uniformly rotating superfluid,[5] and that other phenomena involving vorticity (such as critical velocities) are at least in qualitative agreement with its predictions.[6,7]

The proposition that quantized vortex lines interact with each other according to classical hydrodynamics has been the basis for several discussions concerned with the behavior of large numbers of lines,[7–9] but direct evidence for such an assumption has been meager. Primarily, this is because the detailed behavior of such a complicated system is very difficult to investigate theoretically or experimentally. The discovery of quantized vortex rings by Rayfield and Reif[10,11] has made more precise studies possible since the vortex ring is a simple system whose properties are easily measured. Of particular interest to us is their finding that the motion of a ring is in accord with the predictions of ideal-fluid theory. Since the self-induced velocity of an unconstrained curved vortex filament depends primarily on the local shape of the filament,[12] there is no qualitative difference between the self-induced motion of rings and lines. Thus, Rayfield and Reif's result leads us to expect that at least the self-induced motion of any quantized vortex line will be classical.

An obvious extension of these ideas is to look at the motion of a ring in the presence of other lines or rings, and to compare the observations with the predictions of ideal-fluid dynamics. In this paper we report the results of one such investigation, carried out by looking at the behavior of vortex rings in rotating He II. Some of the experimental results have been published previously.[13] Gamota and Sanders[14] have reported on an alternative approach in which they measure the interaction between positively and negatively charged beams of rings. Their findings and ours should prove complementary.

Our experiment consists of sending a horizontal beam of charged quantized vortex rings across the array of vertical quantized vortex lines presumed to exist in the rotating superfluid. Details of how the lines are arranged are uncertain, but it is generally assumed that they are distributed in such a way that the average velocity field is that of solid-body rotation. The spacing between the lines is of order $(\kappa/\Omega)^{1/2}$, where $\kappa=h/m$ is one quantum of circulation. At a typical angular velocity $\Omega=1$ rad/sec, this gives a spacing of $\sim 10^{-2}$ cm. Since the radii of the rings in the beam are less than $\sim 10^{-4}$ cm, we expect qualitatively that the rings will spend almost all of their time far away from any vortex line, subject only to the average long-range influence of the array. On a purely geometrical basis, we thus expect to see a combination of two effects: violent ring-line encounters characterized by an effective width roughly equal to the diameter of the ring, plus possible long-

† Submitted in partial fulfillment of the requirements for the degree of Doctor of Philosophy at the University of Chicago.

[1] E. P. Gross, Nuovo Cimento **20**, 454 (1961).

[2] L. P. Pitaevskii, Zh. Eksperim. i Teor. Fiz. **40**, 646 (1961) [English transl.: Soviet Phys.—JETP **13**, 451 (1961)].

[3] P. C. Hohenberg and P. C. Martin, Ann. Phys. (N. Y.) **34**, 291 (1965).

[4] A. L. Fetter, Phys. Rev. **151**, 100 (1966).

[5] For an extensive review of these properties, see E. L. Andronikashvili and Yu. G. Mamaladze, Rev. Mod. Phys. **38**, 567 (1966).

[6] R. P. Feynman, in *Progress in Low Temperature Physics*, edited by C. J. Gorter (North-Holland Publishing Company, Amsterdam, 1955), Vol. I, p. 1.

[7] W. F. Vinen, in *Progress in Low Temperature Physics*, edited by C. J. Gorter (North-Holland Publishing Company, Amsterdam, 1961), Vol. III, p. 1.

[8] A. L. Fetter, P. C. Hohenberg, and P. Pincus, Phys. Rev. **147**, 140 (1966).

[9] V. K. Tkachenko, Zh. Eksperim. i Teor. Fiz. **50**, 1573 (1966) [English transl.: Soviet Phys.—JETP **23**, 1049 (1966)].

[10] G. W. Rayfield and F. Reif, Phys. Rev. Letters **11**, 305 (1963).

[11] G. W. Rayfield and F. Reif, Phys. Rev. **136**, A1194 (1964).

[12] R. J. Arms and F. R. Hama, Phys. Fluids **8**, 553 (1965).

[13] K. W. Schwarz and R. J. Donnelly, Phys. Rev. Letters **17**, 1088 (1966).

[14] G. Gamota and T. M. Sanders, Jr., Bull. Am. Phys. Soc. **11**, 361 (1966).

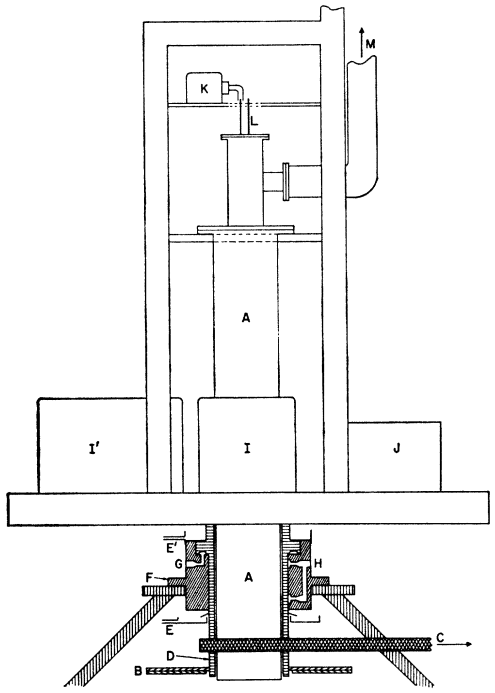

FIG. 1. Schematic of the experimental setup. The Dewar A extends through the journal D. The journal turns in the housing F, and is driven by means of the timing belt C which is connected through a Graham variable-speed transmission to a synchronous motor. Other components are discussed in the text. The plumbing for the He^3 refrigerator has been omitted for the sake of clarity.

range effects which act on every ring in much the same way. With current densities of order 10^{-13} A/cm^2, the average distance between rings in our beam is at least 10^{-2} cm. At long distances, the velocity field of a ring drops off like that of a dipole. Hence for our system, ring-ring effects should be small compared to ring-line effects.

Viewed as a scattering experiment, our procedure is subject to severe limitations which prevent observation of any but the crudest effects. Most of the difficulties trace to the fact that the source and detector are perforce located inside the scattering medium, which is limited in size. For example, it is not possible to create a very well-defined "incident beam" since the collimating region must be kept small compared to the drift-space length of 2.3 cm. Nevertheless, some interesting effects are observed which can be interpreted in terms of the qualitative picture given above. The more detailed theoretical analysis given in Sec. IV yields fair agreement with experiment, although some significant differences seem to exist.

II. APPARATUS

Our experiment required that a large container of liquid helium be rotated while its temperature be kept near 0.3°K. An additional problem was posed by the necessity of extracting from the rotating system at least one, and preferably several, signal currents on the order of 10^{-13} A. A simple solution of the problems presented by these requirements was found by mounting a complete He^3 refrigerator, along with the low-level electronics, on a large turntable.[15] This arrangement did not require sophisticated cryogenic engineering and had the further advantage of being experimentally very flexible. Its main disadvantage was a rather high vibration level due to the mechanical pumps mounted on the turntable. Fortunately, the measurements were not sensitive to variations in temperature, and could be made with the pumps shut off and the temperature drifting. No doubt a better approach would have been to use a He^3 refrigerator which employed only diffusion pumps once it had reached the operating temperature.

The general layout of the apparatus is sketched in Fig. 1, which includes a cut-away view of the large hydraulic bearing in which the table turns. A pump furnishes a continuous flow of oil under pressure to the thrust and centering pads (G,H). After squeezing out past the bearing surfaces, the oil is returned to the pump reservoir by a sump pump connected to E, E'. In operation, the journal is lifted about $\frac{1}{8}$ in. by a thrust pressure of 45 lb/in^2, and is kept on axis by a pressure of 250 lb/in.^{2} applied through restrictors to 12 centering pads such as H. This arrangement automatically keeps the table centered to a high degree of accuracy.

The He^3 refrigerator closely resembled that used by Reif and Meyer,[16] differing mainly in that our volume of cooled liquid (300 cc) was considerably larger. Under ideal conditions, a temperature of about 0.31°K could be obtained, although most of the data were taken at 0.4°K. All of the necessary pumps (I,I') were mounted on the table except the one for the main He^4 bath (M). The bath was pumped from off the table through a 4-in. rotating vacuum seal which will be described in detail elsewhere.[15] It is perhaps worth noting that electrical feedthroughs made by using Stycast epoxy[17]

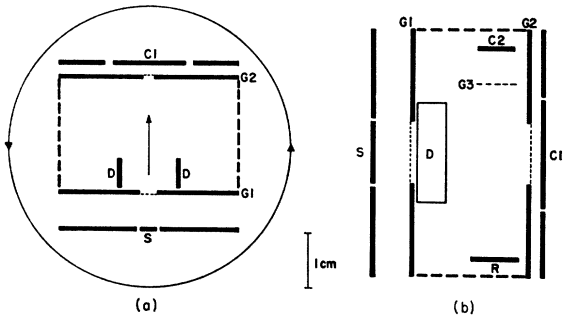

FIG. 2. Top (a) and side (b) views of the experimental cell.

[15] A technical description of the turntable, rotating vacuum seal, and rotating electrical contacts will be published.
[16] F. Reif and L. Meyer, Phys. Rev. 119, 1164 (1960).
[17] K. S. Balain and C. J. Bergeron, Rev. Sci. Instr. 30, 1058 (1959).

proved to be absolutely reliable at low temperatures, whereas considerable trouble was encountered in using commercial glass-to-metal seals.

All electrical signals, bias voltages, and power to the table passed through rotating contacts (B). Each of these (24 in all) consisted essentially of a circular copper wiper rotating in a fixed Lucite groove filled with mercury. The measured noise generated by these contacts during rotation was less than 1 μV into an impedance of 5 kΩ. The signal currents were fed from the experimental cell to the top of the Dewar by two coaxial leads (L) and detected by a Model 31 Cary vibrating-reed electrometer (J,K). The low- and high-level outputs of the electrometer were then fed into an Azar strip chart recorder and a Mosely X-Y recorder, respectively.

Temperature was measured and controlled by a slightly modified version of the phase-sensitive bridge circuit of Blake and Chase.[18] The sensing element was a 470-Ω, grade-1002, $\frac{1}{2}$-W Speer resistor; and the controlling element was a 10-Ω Nichrome wire heater. A rough calibration of the resistor against the He^3 vapor pressure was considered sufficient since our results were not sensitive to temperature changes. Good agreement was obtained with the resistance curve given by Black *et al.*[19]

III. MEASUREMENTS

Most of our data were taken with the cell shown in Fig. 2, which is drawn approximately to scale. The 10 μ Ci Po^{210} source S[20] produces ions of both signs, and some of these are accelerated to form rings by a voltage V_1 applied between G1 and S. To assure a good field configuration, S is closely surrounded by a guard plate and the opening in G1 is covered by a fine-mesh screen. The deflection plates D allow us to look at the beam of rings by sweeping it across the narrow opening in G2. A calibration of deflection as a function of applied voltage and ring energy was obtained with a split collector similar to that used by Rayfield and Reif.[11] The deflection angle (in radians) can be written as $\Delta\theta=\alpha\Delta V/V_1$, where $\alpha=1.3\pm0.2$, and ΔV is the voltage applied across the deflection plates. Allowing for the difference in geometries, this is in reasonable agreement with the results of Rayfield and Reif. Once the rings have passed through the drift region G1-G2, a back voltage V_2 may be applied between G2 and the collector C1 to analyze their energy. The drift space was enclosed on all sides by a shield connecting G1 and G2 so that only the deflection fields acted on the rings. The side view in Fig. 2(b) also shows the repeller R, a second collector C2, and a third grid G3 which were later added to look for charges trapped in the lines.

[18] C. Blake and C. E. Chase, Rev. Sci. Instr. 34, 984 (1963).
[19] W. C. Black, Jr., W. R. Roach, and J. C. Wheatley, Rev. Sci. Instr. 35, 587 (1964).
[20] The source was very kindly loaned to us by Professor L. Meyer.

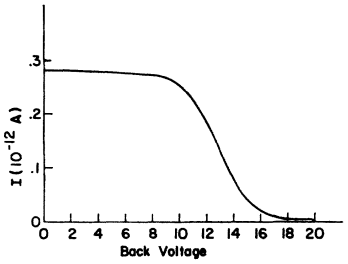

FIG. 3. Typical scan of current collected at C1 versus back voltage V_2. For this curve eV_1 was 20 eV.

A typical scan of collected current versus V_2 is shown in Fig. 3. One worrisome aspect of such scans is that the ring current is gradually cut off at a back-voltage considerably below V_1, whereas the ideal behavior would be a sudden drop at $V_2=-V_1$. Similar effects have been observed by others.[21] We wish to point out, however, that the shape of the cutoff spectrum may be very sensitive to details of grid alignment and beam spread. It is easy to show (see Appendix A) from the ideal equations for the ring motion,[11] that if a ring of energy eV_1 comes into a region of retarding potential at a small angle β to the normal, the back voltage necessary to prevent it from reaching the collector is given by $V_2=-V_1(1-\beta^{1/2})$. A deviation of only 0.04 rad will decrease the apparent energy by 20%. Hence a small angular spread in the beam when it arrives at G2 will smear out the cutoff scan toward lower energies, while misalignment of the grids will move the cutoff itself to significantly lower energies. One does not expect this argument to provide an exact explanation of Fig. 3, since other effects such as nonuniformity of the field near the screens, space charge, and ring-ring interactions may play important parts, but it certainly indicates that the back-voltage method is not a very good way to measure ring energies. Since Rayfield and Reif obtained excellent agreement with theory by assuming the true energy of the rings in their drift space to be just eV_1, we shall analyze our results in terms of this assumption, with the reservation that it represents an upper limit.

When the beam was scanned by means of the deflection plates, it was found to be quite broad (see Fig. 4). Details in the shape of the beam varied from run to run, but average properties such as width and amplitude were repeatable. Our experience indicates that most of the variations were caused by surface charge on the electrodes. Because of the rather large angles and fields involved, the scans probably do not give an accurate picture of the beam at its outer edges, and we confine most of our attention to the region around the maximum.

When the system is set into rotation, the scans vary with Ω as shown in Fig. 4. The primary effects of the

[21] G. W. Rayfield, thesis, University of California, Berkeley, 1964 (unpublished).

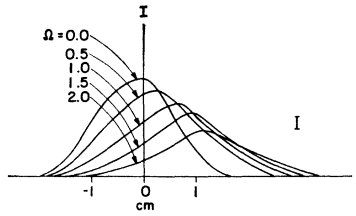

FIG. 4. Beam shape at the collector as a function of Ω (rad/sec). The current I is in arbitrary units. The bar at the right indicates the noise which has been smoothed out in drawing these scans.

rotation are a decrease in the intensity of the collected current and a shift in the position of the whole beam at the collector. Some change in the shape of the beam is usually also observed. In the light of the previous discussion, it is natural to analyze the observed loss of intensity in terms of close encounters between rings and lines. Thus, assuming a uniform density of vortex lines $2\Omega/\kappa$, one expects the intensity to vary as

$$I=I_0\exp\{-(2\Omega/\kappa)l\sigma(eV_1)\},$$

where l is the distance across the drift space and $\sigma(eV_1)$ is the effective width of a line for removal of an incident ring from the beam. In Fig. 5 we show plots of I versus Ω for representative values of eV_1. The fact that they all exhibit the predicted exponential dependence is solid evidence that the effective width is a meaningful and well-defined quantity. Its values can be determined from the slopes of the plots shown in Fig. 5, and the results of our measurement are given in Fig. 6. These values are somewhat smaller than the preliminary results reported previously.[13] The difference arises from the fact that the earlier points were taken with $V_2\cong-0.5V_1$, in order to make sure of seeing only rings, while the data in Fig. 6 were taken with $V_2=0$. When the system is rotating, the rings come into the G2-C1 region at an angle β to the normal which increases with Ω. As we have seen above, this can result in an extra decrease in the collected current and hence a spuriously high σ. The points taken with $V_2=0$ do not suffer from this source of error.

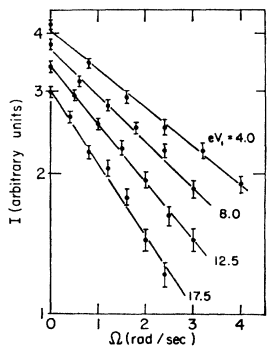

FIG. 5. Collected current at the maximum versus speed of rotation for different ring energies.

Since to first order all rings in the collected beam seem to have undergone the same deflection, it is likely that this effect arises from the averaged long-range action of the lines. The shift of the beam was always found to be opposite to the direction of rotation [i.e., to the right of the arrow in Fig. 2(a)]. Its dependence on Ω was accurately linear, as seen in Fig. 7. Plotting the slopes of such curves versus the inverse of the ring velocity in Fig. 8, one sees a close proportionality for $eV_1<20$ eV. It should be noted that the quantity measured is not the actual displacement at the collector but the value of ΔV across the deflection plates necessary to bring the center of the beam back to the hole in the collector. As shown schematically in Fig. 9, this means that the beam is started out at a known small angle α; and when we speak of shifts, the implicit assumption is that the two paths in Fig. 9 are affected in nearly the same way

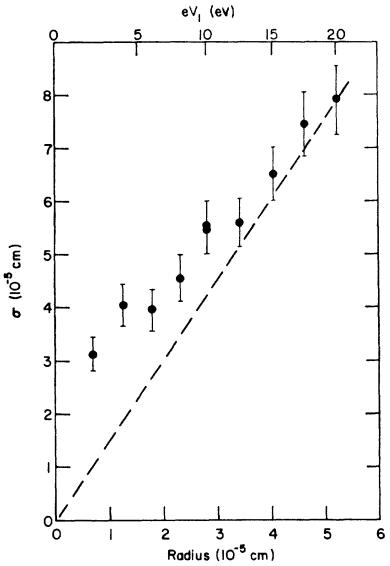

FIG. 6. Effective widths as a function of ring radius. The error bars represent the uncertainties in estimating σ from data such as that of Fig. 5. The dashed line is the theoretical prediction derived in Sec. IV.

by the average velocity field. As long as we confine ourselves to small deflections, this assumption is reasonable and allows us to take $BC=AB$.

To recapitulate, our data are rather crude because of difficulties inherent in the experiment, but they do yield an effective width which seems to result from local ring-line interactions. They also show the existence of large deflections, experienced by the beam of rings as a whole and closely proportional to Ω/U, where U is the ring velocity corresponding to eV_1. No dependence on the charge of the rings or on temperature was observed below 0.5°K, in agreement with a purely hydrodynamic model.

Of considerable interest is the question of what happens to the rings which disappear from the beam.

The scans in Fig. 4 do not show any evidence of significant scattering in the plane perpendicular to the rotation axis. However, large rotation-dependent currents were observed at the collector C2 [see Fig. 2(b)]. The variation of these currents with Ω was quantitatively consistent with the idea that any charge lost by the beam moves mainly in the vertical direction. For a narrow collector C2, such a simple model predicts a current proportional to $\Omega \exp\{-2\Omega l'\sigma/\kappa\}$, and this describes our observations quite well. This expression was in fact applied to traces of I_2 versus Ω to obtain σ and the resulting values agreed well with the more accurate determinations of Fig. 6.

The back voltage on R necessary to stop any current from reaching C2 corresponded to a field of less than $\sim$0.3 V/cm. This gives a rough estimate of the space-charge fields existing in the drift region, and they are seen to be quite small. Because the vertical current is stopped so easily by a reverse bias on R, it appears likely that it consists of charges trapped in vortex lines.[22,23] To test this further, a wide-meshed screen G3 was placed in front of C2. Even when a large forward

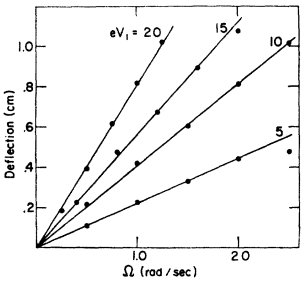

FIG. 7. Deflections of the beam maximum at the collector as a function of angular velocity.

voltage was applied between the two, no upward current could be detected. This kind of behavior is quite characteristic of charges trapped in lines,[24] the lines preferring to terminate on the grid wires rather than pass near by them. Rings, of course, pass through coarse screens with ease. The trapping of positive charges by the vortex lines has not been observed previously, but its occurrence at low temperatures is in agreement with the theoretical prediction of Donnelly.[25]

If a large enough ($\sim$2 V/cm) upward field was applied to the R-G3 region, it *was* possible to observe an upward current which increased with Ω. This current behaved as though composed of rings, in that a back voltage on C2-G3 about equal to the forward voltage on R-G3 was required to stop it. This indicates that after the charge is lost from the beam, it probably

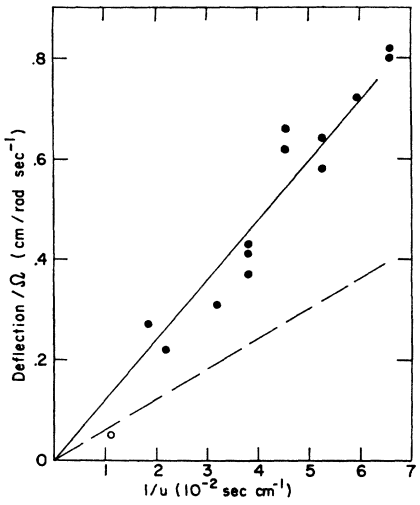

FIG. 8. Slopes of the deflection versus Ω curves as a function of $1/U$. The solid line is drawn to fit the data; the dashed line is the theoretical estimate derived in Sec. IV.

spends some time in the fluid, subject to the competitive actions of the lines and the electric field.

Thus our qualitative picture of what happens when a charged ring comes very close to a line is that the charge is released into the liquid, perhaps through the hydrodynamic destruction of the ring and the line. The free charge will either be trapped in a line or create another ring, depending on the size of the electric field acting on it. Once it is trapped in a line, it is constrained to move vertically.

IV. HYDRODYNAMIC CALCULATIONS

In accordance with the discussion in the Introduction, we attempt in this section to see how far the theory of a perfect fluid[26] will go towards explaining the results of our experiment. Quantized vortex lines are true singu-

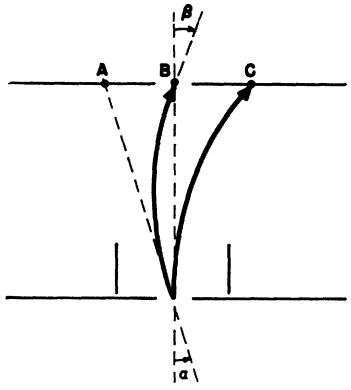

FIG. 9. Schematic representation of "deflection" measurements. Without any deflecting field, the rings arrive at C. We measure the field necessary to bring the beam maximum back to B.

[22] R. L. Douglass, Phys. Rev. Letters **13**, 791 (1964).
[23] B. E. Springett, D. J. Tanner, and R. J. Donnelly, Phys. Rev. Letters **14**, 585 (1965).
[24] J. J. Domingo (private communication).
[25] R. J. Donnelly, Phys. Rev. Letters **14**, 39 (1965).
[26] See, for example, H. Lamb, *Hydrodynamics* (Dover Publications, Inc., New York, 1945).

larities on the hydrodynamic scale, and should therefore represent a realization of the classical vortex-filament concept. The motion at any point $\mathbf{r}$ of an ideal fluid containing such filaments is given in terms of the velocity induced there by the vorticity in the rest of the fluid, according to the Biot-Savart equation

$$\mathbf{v}(\mathbf{r},t)=\frac{\kappa}{4\pi}\int_L \frac{d\mathbf{r}'\times(\mathbf{r}-\mathbf{r}')}{|\mathbf{r}-\mathbf{r}'|^3}, \tag{1}$$

where the line integral is over all vortex filaments and κ is the quantized circulation h/m. The motion of the filaments themselves is then determined by the dynamical requirement that they move with the fluid. As has recently been pointed out by several authors,[8,27] concepts such as the Magnus force and the vortex line tension need not enter the discussion.

Although the theory takes such a physically simple form, actual calculations of the development in time of some initial configuration of vortex lines tend to become very complicated. Much work has been done on the stability with respect to small perturbations of certain symmetrical configurations such as single straight vortex lines,[28] regular arrays of straight vortex lines,[8,9] and vortex rings.[29] The behavior of isolated lines and rings subject to large initial deformations has been investigated by Arms and Hama[30,31] by means of direct numerical integration. Our particular approach is partially based on the formalism of J. J. Thomson's impressive treatise, and we shall make use of some of his results.

The specific problem is to find the effect of an array of vertical vortex lines on the horizontal motion of a vortex ring. Since the ring is small compared to the spacing between the lines, details of the array structure should not be very important. We develop a description of the motion of a ring, as it approaches a single line, which remains valid until the distance from the line to the nearest edge of the ring is less than the radius of the ring. At distances closer than this, the edge of the ring and the line interact approximately like two curved vortex filaments. Thus the ring starts out a long way from the line with "impact parameter" p, defined as the closest distance of approach of the center of the ring to the line if there is no interacton. The long-range theory gives the change in the properties of the ring as it approaches the line. When it is very close, these properties determine the initial conditions for the short-range calculation. The subsequent motion of the near edge of the ring then indicates how violently the ring is being distorted as it passes by the vortex line. Even though this whole procedure is quite crude, it does provide a good idea of the range of impact parameters which result in large distortions, and it shows the nature of these deformations. To discuss possible collective effects on the motion of the rings, we sum the long-range formulas over the whole array of lines.

The time rate of change in the shape of a vortex filament $\mathbf{r}(s,t)$ is $\mathbf{v}(\mathbf{r}(s,t))$, where $\mathbf{v}$ must be computed from the instantaneous configuration of vortex lines according to Eq. (1). Here s is the arc length parameter. In considering the motion of a given filament, one must remember that $\mathbf{v}$ is composed of the velocity field of all the other lines acting at $\mathbf{r}(s,t)$, plus a self-induced velocity. This separation is useful because a simple expression for the self-induced motion exists,[31] viz.,

$$\frac{\partial\mathbf{r}(s,t)}{\partial t}=\frac{\kappa}{4\pi}\mathbf{t}\times\mathbf{C}\left\{\left(\ln\frac{1}{|\mathbf{C}|a}\right)+O(1)\right\}, \tag{2}$$

where $\mathbf{t}$ is the unit tangent to the line in the direction of the circulation, $\mathbf{C}$ is its vector curvature $\partial^2\mathbf{r}/\partial s^2$, a is a cutoff parameter roughly corresponding to the small but finite radius of the filament core, and $O(1)$ represents terms of order 1 contributed by long-range effects. By neglecting the long-range terms we introduce errors of order 10% or less in our case. The motion of the line is thus determined by the velocity field of the ring plus an approximate distortion term arising from Eq. (2). Similarly, the development of the ring depends on the line velocity field plus self-induced terms.

Motion of the Ring

If we use the coordinate system of Fig. 10, a point on the undisturbed ring can be specified by the position of its center $\mathbf{r}_0$, its average radius R, the normal to its plane $\mathbf{h}$, and an angle ψ around the ring which we define with respect to the intersection of the x-y plane and the ring as shown. The x-y symmetry plane is perpendicular to the undisturbed line and passes through the center of the ring. We take, after Thomson, the distortions of the ring to be written as

$$\Delta_R=\sum_{n=1}^{\infty}(\alpha_n\cos n\psi+\beta_n\sin n\psi), \tag{3a}$$

$$\Delta_h=\sum_{n=1}^{\infty}(\gamma_n\cos n\psi+\delta_n\sin n\psi), \tag{3b}$$

where Δ_R is the radial distortion and Δ_h is the displacement along the normal. By symmetry, $\beta_n=\delta_n=0$. As is shown by Thomson, the effect of the ring on itself produces a steady motion along $\mathbf{h}$ with velocity

$$u=\frac{\kappa}{4\pi R}\left\{\ln\frac{8R}{a}-\frac{1}{4}\right\}, \tag{4}$$

and an interaction between the distortion amplitudes

[27] E. S. Raja Gopal, Ann. Phys. (N. Y.) **29**, 350 (1964).
[28] Lord Kelvin, *Mathematical and Physical Papers* (Cambridge University Press, Cambridge, England, 1880), Vol. 4, p. 152.
[29] J. J. Thompson, *A Treatise on the Motion of Vortex Rings* (Macmillan and Company, Ltd., 1883).
[30] F. R. Hama, Phys. Fluids **6**, 526 (1963).
[31] R. J. Arms and F. R. Hama, Phys. Fluids **8**, 553 (1965).

given by ($n>1$)

$$d\alpha_n/dt=-n^2L\gamma_n, \tag{5a}$$

$$d\gamma_n/dt=(n^2-1)L\alpha_n, \tag{5b}$$

where $L=(\kappa/4\pi R^2)\ln 8R/a$. The $n=1$ terms do not interact. All of these statements are valid to order α_n/R, γ_n/R.

To find the effect of the line velocity field $\mathbf{v}_l$, we Fourier-analyze it around the ring

$$\mathbf{v}_l(\psi)=\mathbf{V}_0+\sum_{n=1}^{\infty}\mathbf{V}_n\cos n\psi, \tag{6}$$

where the Fourier coefficients $\mathbf{V}_i$ depend on $\mathbf{r}_0$, $\mathbf{h}$, R, etc. The first term contributes to the motion of the ring as a whole so that, including the self-induced velocity given in Eq. (4),

$$d\mathbf{r}_0/dt=\mathbf{V}_0+\mathbf{h}U. \tag{7}$$

Taking the normal component of the remaining terms and equating it to $d\Delta_h/dt$, we obtain for the action of the line field

$$d\gamma_n/dt=\mathbf{V}_n\cdot\mathbf{h}. \tag{8}$$

A little consideration will show that the γ_1 term corresponds to a tilting of the whole ring rather than a true distortion, so that

$$\frac{d\mathbf{h}}{dt}=-(\mathbf{h}\times\hat{z})\frac{\mathbf{V}_1\cdot\mathbf{h}}{R}, \tag{9}$$

where $\hat{z}$ is the unit vector in the z direction. Higher-order terms develop according to

$$d\gamma_n/dt=\mathbf{V}_n\cdot\mathbf{h}+(n^2-1)L\alpha_n. \tag{10}$$

The tangential component, parallel to the $\psi=0$ axis of the ring, is $(h_y, -h_x)$ dotted into the sum in Eq. (6). In order to discuss radial distortions, we can multiply the tangential component by $\cos\psi$ to obtain to order α/R

$$\begin{aligned}\frac{d}{dt}(R+\Delta_R)&=\cos\psi\{(\mathbf{h}\times\hat{z})\cdot\sum_{n=1}^{\infty}\mathbf{V}_n\cos n\psi\}\\&=\tfrac{1}{2}(\mathbf{h}\times\hat{z})\cdot\{\mathbf{V}_1+\mathbf{V}_2\cos\psi\\&\qquad+\sum_{n=2}^{\infty}(\mathbf{V}_{n-1}+\mathbf{V}_{n+1})\cos n\psi\}.\end{aligned} \tag{11}$$

Hence,

$$dR/dt=\tfrac{1}{2}(\mathbf{h}\times\hat{z})\cdot\mathbf{V}_1, \tag{12}$$

$$d\alpha_1/dt=\tfrac{1}{2}(\mathbf{h}\times\hat{z})\cdot\mathbf{V}_2, \tag{13}$$

$$d\alpha_n/dt=\tfrac{1}{2}(\mathbf{h}\times\hat{z})\cdot(\mathbf{V}_{n-1}+\mathbf{V}_{n+1})-n^2L\gamma_n. \tag{14}$$

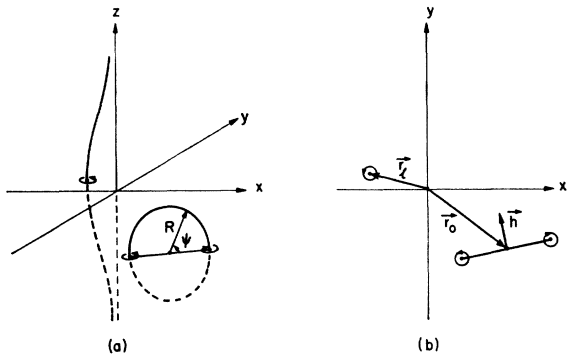

FIG. 10. Coordinate system used in discussing interaction of a ring and a line. A perspective view is given in (a); (b) shows a cut along the symmetry plane.

Motion of the Line

The equations derived above describe the ring motion in terms of the $\mathbf{V}_n$'s, which, of course, depend on the instantaneous shape and position of the vortex line as well as the ring. In treating the long-range interaction of the ring-line system, our basic approximation is to neglect the effect of higher-order distortions in determining the long-range velocity fields. Thus, we shall only use the average properties of the ring $\mathbf{r}_0$, $\mathbf{h}$, and R to work out the motion of the line. In the same spirit, the velocity field exerted by the line is approximated as the field of an undisturbed line located at $\mathbf{r}_l$ in Fig. 10. This is well justified *a posteriori* since our calculations show that, as the ring comes in on the line, $|\mathbf{r}_0-\mathbf{r}_l|$ is always much smaller than the radius of curvature of the line. As far as the motion of the line is concerned, the main quantity of interest is thus the point $\mathbf{r}_l$ at which it cuts the x-y plane.

The effect of the ring field $\mathbf{v}_R(\mathbf{r})$ on the part of the line near the x-y plane is formally simple, although the complicated behavior of $\mathbf{v}_R(\mathbf{r})$ makes actual calculations messy. Expanding about the point $\mathbf{r}_l$ (where the line cuts the x-y plane),

$$\mathbf{v}_R(\mathbf{r}_l,s)=\mathbf{v}_R(\mathbf{r}_l,0)+\left.\frac{\partial\mathbf{v}_R}{\partial s}\right|_{s=0}s+\frac{1}{2}\left.\frac{\partial^2\mathbf{v}_R}{\partial s^2}\right|_{s=0}s^2+\cdots, \tag{15}$$

where s is the arc length along the line. The first term on the right gives the velocity which the ring imposes on the section of line near $\mathbf{r}_l$, the second term has no components normal to the line, and the third term gives the rate at which the curvature of the line changes near $\mathbf{r}_l$.

The self-induced motion of the line is given by Eq. (2), and we can write at once

$$\frac{d\mathbf{r}_l}{dt}=\mathbf{v}_R(\mathbf{r}_l,0)-\frac{\kappa}{4\pi}(\mathbf{C}\times\hat{z})\ln\frac{1}{|\mathbf{C}|a}, \tag{16}$$

where $\mathbf{C}$ is the vector curvature of the line at the x-y plane. $\partial\mathbf{C}/\partial t$ depends not only on the ring field, but also includes a self-induced term. A difficulty arises in

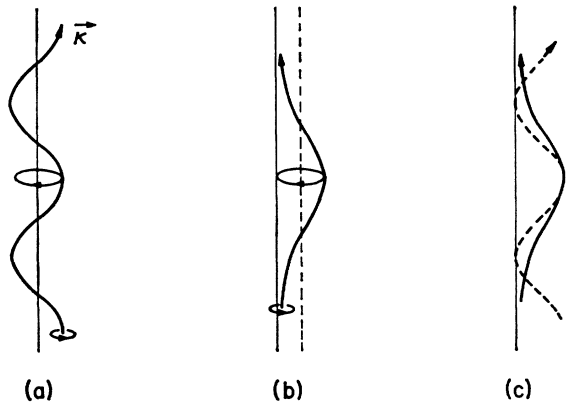

FIG. 11. (a) shows the typical behavior of a sinusoidally perturbed line. In (b) the dashed line is our estimate for the effective rotation axis of the maximum of the perturbed line. (c) illustrates the assumption made in fitting the actual case to a linearized solution.

trying to find the self-induced correction, since this requires knowledge of higher-order distortion terms. Thus differentiating Eq. (2) twice with respect to s, we obtain

$$\frac{\partial \mathbf{C}}{\partial t}=\beta\left(\mathbf{C}\times\frac{\partial \mathbf{C}}{\partial s}+\mathbf{t}\times\frac{\partial^2\mathbf{C}}{\partial s^2}\right), \tag{17}$$

where $\beta=\kappa/4\pi\ln(1/a|\mathbf{C}|)$, and we have neglected the very small variation of the logarithm with s. $\partial\mathbf{C}/\partial s$ and $\partial^2\mathbf{C}/\partial s^2$ depend on the time integral of still higher-order terms which cannot be conveniently calculated. We therefore adopt the expedient of estimating $\partial\mathbf{C}/\partial t$ from the small-perturbation solution of Eq. (2). Setting $s=z$, the exact solutions of the linearized equation have the form[30]

$$\begin{aligned} x&=-A\cos kz\cos(\beta k^2 t), \\ y&=+A\cos kz\sin(\beta k^2 t). \end{aligned} \tag{18}$$

This exhibits a steady retrograde rotation of the plane of the disturbance about the points of inflection of the line [see Fig. 11(a)], a general effect arising from the second term of Eq. (17). If we know $\mathbf{C}$, we know the self-induced velocity at $\mathbf{r}_l$; and we estimate the effective point of inflection ($\mathbf{C}=0$) of the disturbed line to lie about halfway between the unperturbed axis and $\mathbf{r}_l$ [see Fig. 11(b)]. Unless the line is strongly distorted, this cannot in any case lead to any great errors. Essentially, $d\mathbf{C}/dt$ is estimated by looking at the behavior of that linearized solution which has the same curvature at the maximum and the same total excursion as the distorted line [see Fig. 11(c)]. The deviation between the two at large z is of course unimportant, since long-range effects are small.

The rather severe approximation made above enables us to write finally

$$\frac{d\mathbf{C}}{dt}=\left.\frac{\partial^2\mathbf{v}_R}{\partial s^2}\right|_{s=0}+(\mathbf{C}\times\hat{z})\frac{|\mathbf{C}|}{|\mathbf{r}_l|}\left\{\frac{\kappa}{2\pi}\ln\frac{1}{|\mathbf{C}|a}\right\}. \tag{19}$$

Short-Range Equations

When the edge of the ring is less than R from the line, we approximate the motion as that of two curved vortex filaments. Fixing our attention again on the position of the line and the nearer ring edge in the x-y symmetry plane, we find

$$\frac{d\mathbf{r}_R}{dt}=\frac{\kappa}{2\pi}\frac{\mathbf{t}_l\times(\mathbf{r}_R-\mathbf{r}_l)}{|\mathbf{r}_R-\mathbf{r}_l|^2}+\frac{\kappa}{4\pi}\mathbf{t}_R\times\mathbf{C}_R\ln\frac{1}{|\mathbf{C}_R|a}, \tag{20}$$

$$\frac{d\mathbf{C}_R}{dt}=\frac{\kappa}{2\pi}\mathbf{t}_l\times\left\{\frac{\mathbf{C}_R}{|\mathbf{r}_R-\mathbf{r}_l|^2}-2(\mathbf{r}_R-\mathbf{r}_l)\left[\frac{\mathbf{C}_R\cdot(\mathbf{r}_R-\mathbf{r}_l)}{|\mathbf{r}_R-\mathbf{r}_l|^4}\right]\right\}, \tag{21}$$

where $\mathbf{r}_R$ is the position of the ring edge in the x-y plane, $\mathbf{C}_R$ is its vector curvature there, and similarly $\mathbf{r}_l$ and $\mathbf{C}_l$ for the line. The only vectors not in the x-y plane are the tangents $\mathbf{t}_R$ and $\mathbf{t}_l$, which lie along the z axis. Note that $\mathbf{t}_R$ can be pointed either up or down, depending on which edge of the ring is near the line. The motion of the line is described by a symmetrical pair of equations obtained by interchanging R and l in Eqs. (20) and (21). In writing out these equations, all terms of higher order than the self-induced velocity have been neglected.

The first term in Eq. (20) is just the velocity field of the line (neglecting $\mathbf{C}_l$) acting on the ring edge. The second term is the self-induced velocity at the ring edge, according to Eq. (2). One way of looking at Eq. (21) is as giving the first-order rate of change of a vector located in and moving with the fluid. It will change in length and rotate. From Eq. (21) it is easy to show that

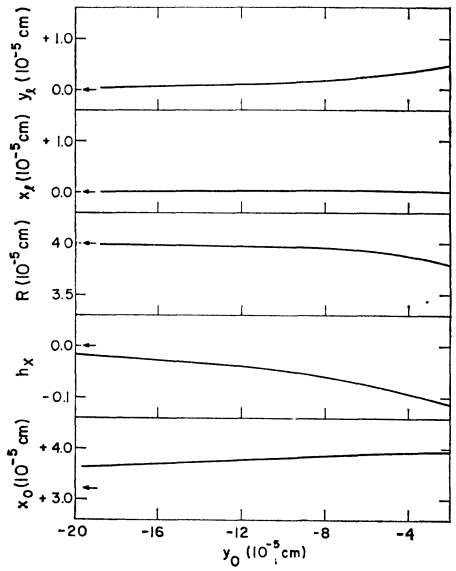

FIG. 12. Computed behavior of ring and line as the ring approaches. The arrows indicate the initial values of the parameters when $y_0=-40\times10^{-5}$ cm. This figure corresponds to an impact parameter of $+3.2\times10^{-5}$ cm.

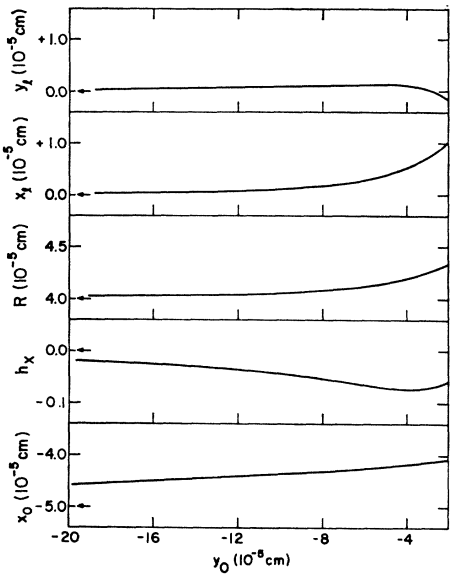

FIG. 13. As in Fig. 12, but with impact parameter -5.0×10^{-5} cm.

the speed of rotation of $\mathbf{C}_R$ in the direction of the line rotation is

$$\omega=\frac{\kappa}{2\pi}\frac{(1-2[\hat{C}_R\cdot\hat{r}]^2)}{\mathbf{r}^2}, \tag{22}$$

where $\mathbf{r}=\mathbf{r}_R-\mathbf{r}_l$ and the circumflexes denote unit vectors. This result is qualitatively useful in showing up the interesting fact that $\mathbf{C}_R$ can be turned in either direction by the line field. It should be noted that because of the drastic influence of $\mathbf{C}_R$ and $\mathbf{C}_l$, Eqs. (20) and (21) and those for the line predict motions which may be quite different from the simple case $\mathbf{C}_R=\mathbf{C}_l=0$.

Numerical Integration

To obtain an estimate of σ, we look for the range of impact parameters which result in strong distortion of the ring. The initial configuration used (see Fig. 10) is a ring with $\mathbf{h}=(0,1)$, $y_0=-10R$, and $x_0=$ impact parameter. The line, of course, is initially located at the origin. The motion of the ring-line system is then determined by numerical integration of the long-range equations developed above.[32] The actual expressions for the $\mathbf{V}_n$'s and the ring velocity field are given in Appendix B. Typical results of the long-range theory for positive and negative impact parameters are shown in Figs. 12 and 13, respectively. In addition to the average properties shown in these figures, we also calculated $\mathbf{C}_l$, α_1, α_2, and γ_2. The curvature of the line was always much less than $1/R$, while the distortions reached at most a few percent of R. This shows that the approximations made in developing the theory are good.

[32] The calculations were performed by means of the IBM 7094 computer at the University of Chicago.

When the ring is close to the line, we take a point on Figs. 12 or 13 as the initial configuration for integration of the short-range equations, and use these to follow the motion of that edge of the ring which is nearest the line. As the initial impact parameter p is varied from large negative to large positive values, four qualitatively different types of behavior are seen. For $p\lesssim-R$, the line dodges around the right edge of the ring as in Fig. 14(a). As the ring is aimed to overlap the line, a point is reached where the line and ring trap each other in a complicated fashion, the line winding itself around the edge of the ring [see Fig. 14(b)]. We take the onset of this phenomenon to mean that the ring is destroyed. For positive impact parameters, the line wants to dodge around the other edge of the ring, as shown in Fig. 15(a). With a decrease in p, the distortion of the line-ring system becomes increasingly violent, as in Fig. 15(b). This also shows up in the calculated values of C_R and C_l, which become very large. The onset of such large distortions is also assumed to result in removal of the ring from the beam.

The results shown in Figs. 12–15 were calculated for the case $R=4\times10^{-5}$ cm, but further computations showed that they scale well with R. On the basis of these results we estimate that the range of impact parameters which result in destruction of the ring is $-R\lesssim p\lesssim0.5R$. This gives a reaction width $\sigma=(1.5\pm0.2)R$, where the uncertainty arises mainly from the fact that the calculations depend somewhat on where the long-range and short-range equations are matched up. Our estimate of σ is shown as a dotted line in Fig. 6, which also contains the experimental data. The fit is fairly good at high energies, but for very small rings there is a definite discrepancy which cannot be explained hydrodynamically.

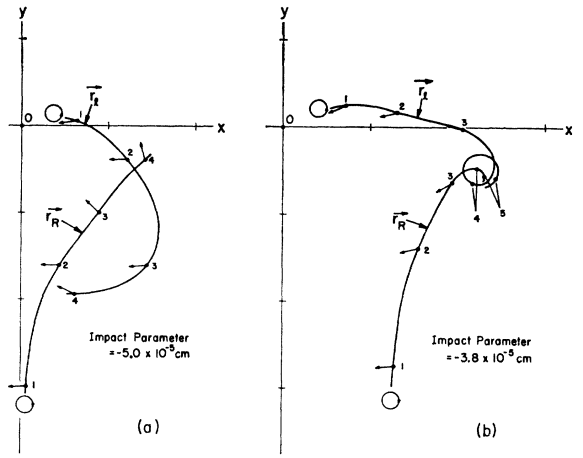

FIG. 14. Computed paths of ring edge and line in units of 10^{-5} cm, for a ring of initial radius 4×10^{-5} cm. Equal numbers are equal points in time. The arrows indicate the directions of the vector curvature, the circles show the sense of circulation. Note that in this figure the plane of the ring extends to the left.

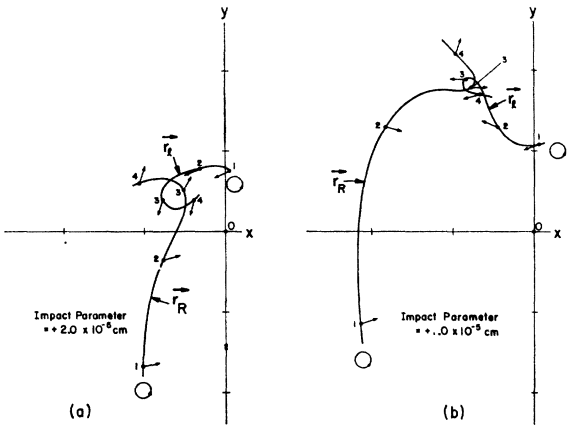

FIG. 15. As in Fig. 14, but for positive impact parameters the plane of the ring extends to the right.

Collective Effects

For the limiting case where the ring-line distance is much greater than the radius of the ring, the equations governing the rate of change of the average properties of the ring simplify to

$$\frac{d\mathbf{r}_0}{dt}=\mathbf{h}U+\frac{\kappa}{2\pi}\frac{(y,-x)}{x^2+y^2}, \tag{23}$$

$$\frac{dh_x}{dt}=\frac{\kappa}{2\pi}\frac{(x^2-y^2)}{(x^2+y^2)^2}, \tag{24}$$

$$\frac{dR}{dt}=\frac{\kappa}{2\pi}\frac{xy}{(x^2+y^2)^2}, \tag{25}$$

where now the ring is situated at the origin with $\mathbf{h}=(0,1)$ and the line is at (x,y). These equations also follow from Thomson's less accurate formulation. When averages are taken over a whole array of lines, quite interesting effects arise. For lack of more precise information, the array is generally assumed to be of uniform density $2\Omega/\kappa$, and to provide an average velocity field closely resembling solid-body rotation. Equation (23) then implies that the instantaneous velocity $d\mathbf{r}_0/dt$ of the ring (in the lab frame) is composed of $U\mathbf{h}$ plus the solid-body velocity at the position of the ring.

The average rate of tilt of the ring has the form

$$\frac{dh_x}{dt}=\frac{\Omega}{\pi}\int_{\text{Array}}\frac{dr}{r}(\cos^2\vartheta-\sin^2\vartheta)d\vartheta, \tag{26}$$

which depends on the shape of the boundaries relative to the position of the ring. Geometries which extend in the plane of the ring give $dh_x/dt>0$, so that the ring tilts opposite to the direction of rotation. If the geometry extends along the normal, the tilt is in the direction of rotation. It is readily seen from Eq. (26) that even for quite bizarre shapes,

$$-\pi\lesssim\int_a\lesssim\pi,$$

and certainly our experimental geometry lies within these limits. The effects on the radius of the ring, found by averaging Eq. (25) over the array, are similar. The largest rate of change of the radius should be observed when the system extends at an angle of 45° to the direction of motion of the ring.

Our observations of the long-range effects (see Sec. III) were byproducts of the effective width measurements, and are hence somewhat crude and unsystematic. On the other hand, the theoretical speculations above can be meaningful only in a qualitative sense, since they are based on what is probably an oversimplified model of the vortex line array. With these reservations in mind, we can at the least conclude that theory and experiment are not inconsistent. If in Fig. 2(a) the center of rotation is located a distance s_1 from G1 and s_2 from G2, the beam at the collector would appear to be shifted owing to three terms: (1) assuming that U is much greater than the velocities due to the rotation, the collector will have moved a distance $+s_2(s_1+s_2)\Omega/U$, with respect to the lab frame, in the time it has taken the ring to cross the distance s_1+s_2; (2) when it arrives, the ring has been swept sideways by the average velocity field through a distance $\frac{1}{2}(s_2^2-s_1^2)\Omega/U$; (3) the plane of the ring has been tilted at some average rate $\sim\beta\Omega$, giving rise to an additional displacement $\frac{1}{2}\beta(s_1+s_2)^2\Omega/U$, where $|\beta|\lesssim 1$. Combining these terms,

$$\text{observed shift}\approx-(\Omega/U)\tfrac{1}{2}(s_1+s_2)^2(1-\beta). \tag{27}$$

In our experiment, $s_1+s_2=2.3$ cm, which gives a maximum deflection of $-5.3\Omega/U$. As seen in Fig. 8, the experimental points fall quite a bit above this slope, but there is order-of-magnitude agreement. In particular, the experimental deflections are closely proportional to Ω/U.

V. DISCUSSION

It appears from the foregoing that large rings are destroyed according to hydrodynamic predictions based on a uniform distribution of quantized vortex lines with density $2\Omega m/h$. In the limit of small rings, the measured effective width for removal from the beam is too large to be explained hydrodynamically. Since our apparatus had a top speed of 4 rad/sec, the percentage decrease in current $\Delta I/I$ due to rotation was small for low-energy rings. It is therefore likely that the deviation arises from some small additional effect which assumes importance as $\Delta I/I\rightarrow 0$. Whether this effect arises from some deficiency associated with the experimental conditions (such as variable surface charges), or from a physically interesting mechanism (such as charge transfer between undisturbed rings and lines) is a

question which requires more detailed investigations of considerable technical difficulty.

The deflections measured are in qualitative agreement with theory, showing a linear dependence on Ω/U. An interesting test of our interpretation of this phenomenon would be to investigate its dependence on the geometry of the drift space. With the proper configuration, one should also be able to observe changes in ring energy arising from Eq. (25).

Finally, we wish to point out that the data presented here provide additional evidence for the quantized vortex line model of rotating He II, in that they are logically interpreted in terms of localized areas in the liquid which strongly affect the ring motion. The large hydrodynamic interaction observed by us indicates that vortex rings will prove a powerful tool with which to investigate the detailed structure of the rotating superfluid, as well as the breakdown of superfluid flow by the creation of quantized vortex lines.

ACKNOWLEDGMENTS

I wish particularly to thank Professor R. J. Donnelly for his advice, encouragement, and support in carrying out this experiment. The construction and maintenance of the apparatus was largely due to the efforts of J. V. Radostitz, A. J. Dudiak, and R. W. Koster. The design for the hydraulic turntable was very kindly provided by E. R. Maki of General Motors Research Laboratories. Useful discussions with Professor D. Fultz and Dr. B. E. Springett are also gratefully acknowledged. This research was supported by the National Science Foundation under Grant GP 5302 and by the Air Force Office of Scientific Research under Grant AF-AFOSR 785-65. We have also benefited from the use of facilities provided by the Advanced Research Projects Agency for materials research at the University of Chicago.

APPENDIX A

According to Rayfield and Reif, the motion of a charged quantized vortex ring is, to a good approximation, given by

$$E=Ap^{1/2}, \tag{A1}$$

$$\dot{p}=e\mathcal{E}, \tag{A2}$$

where E=energy, p="momentum", and $\mathcal{E}$=electric field. Only the component of p parallel to $\mathcal{E}$ will change. The motion of the ring is conservative so that after dropping through a back voltage ΔV, $E=E_0-e\Delta V$, and

$$P_{\parallel}=(E_0-e\Delta V)^4/A^4-P_{\perp}^2, \tag{A3}$$

where $P_{\parallel}$ is the component parallel to the field and $P_{\perp}$ is the constant perpendicular component. The ΔV necessary to bring $P_{\parallel}$ to zero (so that the ring cannot reach the collector) is given by

$$e\Delta V=E_0[1-(P_{\perp}/P_0)^{1/2}], \tag{A4}$$

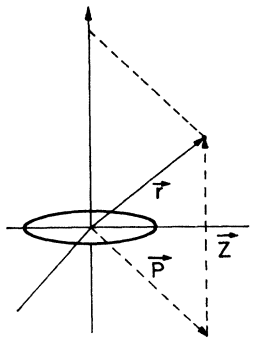

FIG. 16. Coordinate system for Eq. (B4).

where P_0 is the total initial momentum corresponding to E_0. Hence, if a ring of energy E_0 comes into the retarding region at a small angle β to the normal, the stopping potential is given by

$$e\Delta V=E_0(1-\beta^{1/2}). \tag{A5}$$

APPENDIX B

In terms of the coordinate system of Fig. 10, the velocity field of the line is

$$\mathbf{v}(\mathbf{r})=\frac{\kappa}{2\pi}\left\{\frac{-(y-y_l),(x-x_l)}{(x-x_l)^2+(y-y_l)^2}\right\}, \tag{B1}$$

where some of the vectors are written in component notation. A point on the ring has x and y coordinates

$$\mathbf{r}=\mathbf{r}_0+(h_y, -h_x)R\cos\psi. \tag{B2}$$

Under our approximations, the Fourier components determining the ring motion then become

$$\frac{2\pi}{\kappa}\mathbf{V}_n=\frac{2}{\pi}\int_0^{\pi}\frac{(-y'+h_xR\cos\psi,\ x'+h_yR\cos\psi)\cos n\psi d\psi}{(x'+h_yR\cos\psi)^2+(y'-h_xR\cos\psi)^2}, \tag{B3}$$

where $\mathbf{r}'=\mathbf{r}_0-\mathbf{r}_l$, and $\mathbf{V}_0$ contains an extra factor of $\frac{1}{2}$. The $\mathbf{V}_n$'s are treated as parameters which must be reevaluated at each step in the integration.

Using the coordinates of Fig. 16, the velocity field of the ring can be written directly

$$\mathbf{v}_R=(\kappa R/2\pi)\{\hat{P}ZB_1+\hat{Z}(RB_0-PB_1)\}, \tag{B4}$$

where

$$B_n=\int_0^{\pi}\frac{\cos n\vartheta d\vartheta}{(Z^2+P^2+R^2-2PR\cos\vartheta)^{3/2}} \tag{B5}$$

and the circumflexes denote unit vectors. In terms of our system,

$$\begin{aligned} Z&=(\mathbf{r}_l-\mathbf{r}_0)\cdot\mathbf{h},\\ \hat{Z}&=\mathbf{h},\\ P(s)&=(|\mathbf{r}_l-\mathbf{r}_0|^2-Z^2+s^2)^{1/2},\\ \hat{P}(s)&=[1/P(s)]\{\alpha h_yP(0), -\alpha h_xP(0)\ s\}, \end{aligned} \tag{B6}$$

where $\alpha=\pm 1$, depending on whether the ring normal is aiming to the left or the right of $\mathbf{r}_l$. The curvature of the line has been neglected in writing Eqs. (B6). Inserting the expressions in Eqs. (B6) into Eqs. (B4) and (B5), and expanding in powers of s, we obtain, after some complicated arithmetic,

$$\mathbf{v}_R(\mathbf{r}_l,0)=(\kappa R/2\pi)\{(\alpha h_y,-\alpha h_x)ZB_1 + (h_x,h_y)(RB_0-PB_1)\} \quad \text{(B7)}$$

and

$$\left.\frac{\partial^2\mathbf{v}_R(\mathbf{r}_l,s)}{\partial s^2}\right|_{s=0}=\frac{\kappa R}{2\pi}\left\{(\alpha h_y,-\alpha h_x)\left(\frac{3Z}{P}C_1-\frac{Z}{P^2}B_1\right) + (h_x,h_y)\left(\frac{3R}{P}C_0-3C_1-\frac{B_1}{P}\right)\right\}, \quad \text{(B8)}$$

where

$$C_n=\int_0^\pi \frac{(-P+R\cos\vartheta)\cos n\vartheta d\vartheta}{(Z^2+P^2+R^2-2PR\cos\vartheta)^{5/2}}. \quad \text{(B9)}$$

In Eqs. (B7), (B8), and (B9), P is meant to be evaluated at $s=0$.

To check the effect of taking some of the neglected terms into consideration, computations were also carried out using $R+\alpha_1\cos\Psi$ instead of R in Eq. (B3). It was found that this way of taking the first distortion term into account produced a completely negligible correction. A more accurate form of Eqs. (B6) which took account of the line vector curvature near the x-y plane was also tried, and also produced only a small correction. This is consistent with the fact that the radius of curvature of the line was always found to be much greater than the ring-line distance.

Erratum

Forbidden Continuum: Free-Bound Transition in Hydrogen Plasmas, MICHAEL C. WEINBERG AND R. STEPHEN BERRY [Phys. Rev. **144**, 75 (1966)]. A factor of 2π was missing in the expressions for $\sigma(R)$ or for $A(\lambda)$. As a result, the entries in Table I should be 30.2×10^8, 48.4×10^8, 13.2×10^9, and 25.1×10^9. Furthermore, the values in Table II, Figs. 6, and 7 refer to perturber densities of 4×10^{13} ions/cm^3; in Fig. 4, to 2×10^{14} ions/cm^3, and in Fig. 5, to 4×10^{13} ions/cm^3. The corrected values thus show a larger effect due to forbidden continuum than did those originally published.